Mon. Not. R. astr. Soc. (1975) **171**, 555–568.

EVOLUTION OF HELIUM WHITE DWARFS IN CLOSE BINARIES

Ronald F. Webbink

Institute of Astronomy, Madingley Road, Cambridge CB3 0HA

(Communicated by P. P. Eggleton)

(Received 1975 January 2; in original form 1974 November 5)

SUMMARY

Stars of 0·10, 0·15, 0·20, 0·25, 0·35 and 0·50 $M_\odot$ have been evolved from the zero-age main sequence to extinction of the hydrogen-burning shell as a white dwarf, or to the onset of the helium flash. Shell-burning models are discussed as close binary remnants. Only p–p shell burning configurations exist for 0·10 and 0·15 $M_\odot$ stars. More massive stars display strong thermal pulses at the onset of shell degeneracy and at the reversion from CNO-cycle to p–p chain in the shell. All shells are thermally unstable along the white dwarf track; only close binary systems which reach the second period of mass transfer before remnants reach this stage are therefore likely to avoid nova outbursts.

1. INTRODUCTION

It is now well established that helium white dwarfs of low mass are produced in low-mass close binary systems within a cosmological time scale. Refsdal & Weigert (1971) have demonstrated that a simple relationship exists in Case B mass transfer (which begins with a shell-burning primary) between the total mass and angular momentum of the system and the mass of the white dwarf remnant. Mass transfer in Case A closely resembles Case B during the final phases of mass transfer on a nuclear time scale (Ziolkowski 1970), but with smaller, cooler, more degenerate cores.

White dwarfs in close binary systems are frequently invoked as the sites of novae outbursts, which occur when the original secondary overfills its Roche lobe and spills hydrogen-rich material on to a hot, degenerate white dwarf (see, for instance, Rose 1972). Refsdal & Weigert (1970) have constructed linear series of thermal equilibrium models of low mass into the white dwarf region, but only Kippenhahn, Thomas & Weigert (1968) have followed the evolution of a close binary remnant beyond the onset of shell degeneracy, well into the white dwarf region.

This paper presents calculations of the evolution of single, low-mass stars (of insufficient mass to ignite helium) from the shell-burning Hayashi phase to the death of hydrogen burning. These models are discussed within the context of white dwarf remnants in close binary systems, and as they relate to the results previously obtained by Kippenhahn *et al.* (1968).

2. NUMERICAL METHODS

The evolutionary code employed in this study was a development of one kindly lent by P. P. Eggleton. The equation of state is discussed in some detail by Eggleton, Faulkner & Flannery (1973), and the method of solution, which incorporates composition variables into the set of structure variables included in a non-Lagrangian mesh, has been explained by Eggleton (1971, 1972). A weak-screening correction (Frank-Kamenetskii 1962) was applied to the hydrogen-burning reaction rates. Throughout the present study, a mesh function of the form

$$Q = \ln (M + 0{\cdot}005\, M_*) - 0{\cdot}15 \ln P - 0{\cdot}30 \ln (P + 10^{15}) - 0{\cdot}10 \ln T \quad \text{(cgs units)} \quad (1)$$

was chosen, where M, p and T are the local mass, pressure and temperature co-ordinates corresponding to mesh coordinate Q, and M_* is the total mass of the star. Mesh points are automatically distributed at equal intervals of Q. Model atmospheres are included within the Henyey mesh rather than being fitted on to an interior solution.

It should be pointed out here that the effects of crystallization in the cores of these stars have been neglected. The results of Kovetz & Shaviv (1970) indicate that significant fractions of the helium cores of these models should be in the crystalline state, especially at the lower end of the mass spectrum. One can only conjecture at this stage on what effect inclusion of non-ideal ionic effects might have on the general properties of these models, but there are several reasons to suppose that the differences would be minimal. First, the degree of electron degeneracy in the cores of these stars is relatively low, and remains so in time for the lower mass stars. At low degeneracy the heat capacity of the electron gas will still dominate that of the ion gas (or solid). Thus the phase transition is accompanied by a much less dramatic change in thermal properties than in massive, highly degenerate cores. One might suppose that the gravitational luminosity of a crystalline core is somewhat lower than that calculated for the ion gas, but the situation is also somewhat mitigated by the large latent heat released by material crystallizing at the surface of the solid core. In any case, we shall see that the evolution of those stars which should have substantial crystalline cores is determined by the energy output of the hydrogen-burning shell. The helium cores of such stars are virtually isothermal, with the temperature regulated by the shell temperature.

In this study it has been necessary to avoid the use of very small time steps in following the thermal instabilities of hydrogen-burning white dwarfs, as these phases of evolution otherwise become forbiddingly expensive to follow. Such a procedure suppresses the most violent instabilities in a CNO-cycle shell-burning star, but we trust that in so doing the subsequent course of evolution is not significantly affected.

3. INITIAL MODELS

A low-mass zero-age hydrogen-burning main sequence was constructed by removing mass from an initial $0{\cdot}75\ M_\odot$ model and suppressing all energy sources other than nuclear burning. A Population I composition with $X = 0{\cdot}70$, $Y = 0{\cdot}28$, $Z = 0{\cdot}02$ was chosen for this sequence. From this sequence, models of mass $M/M_\odot = 0{\cdot}10$, $0{\cdot}15$, $0{\cdot}20$, $0{\cdot}25$, $0{\cdot}35$ and $0{\cdot}50$ were selected for the present study. These models were evolved through core and shell hydrogen-burning phases. Since, during main-sequence evolution, the surface convective zones of these

stars extend into nuclear burning regions, surface hydrogen depletion becomes very marked for lower masses, a fortuitous coincidence in simulating quite well the surface hydrogen depletion naturally occurring as a result of mass loss in the close binary remnants to which we wish to compare these models.

As the inert degenerate core increases in mass, the shell temperature grows, driving the entropy of the convective envelope upwards until the expansion of the envelope is balanced by decreasing mass content. The radius of the star thus reaches a maximum. For sufficiently massive stars, $M \gtrsim 0{\cdot}4712\ M_\odot$, this process is arrested by the helium flash. Stars in the narrow mass range $0{\cdot}4649\ M_\odot \lesssim M \lesssim 0{\cdot}4712\ M_\odot$ only reach the helium flash during their descent to the white dwarf track. Stars less massive than about $0{\cdot}12\ M_\odot$ decrease in radius throughout the shell-burning stage. These extremes define the upper and lower bounds to what we will term the zero-age remnant (ZAR) sequence, i.e. the shell-burning configuration of maximum radius.

Table I summarizes the properties of stars lying on the ZAR sequence. Plasma neutrino luminosities are tabulated under $\mathscr{L}_\nu$. Envelope masses, $M_{\rm env}$, are computed using the working definition:

$$M_{\rm env} \equiv M - \left(\frac{Y(M)}{X(M)+Y(M)}\right)\int_0^M \left(\frac{Y(m)}{Y(M)} - \frac{X(m)}{X(M)}\right) dm, \qquad (2)$$

TABLE I

Mass	0.10	0.15	0.20	0.25	0.35	0.50
Age (10^9 yr.)	(3178.320)	3571.400	2058.955	1164.180	405.9511	(124.4373)
log ($\mathscr{L}/\mathscr{L}_\odot$)	(-3.2214)	-0.7730	0.4634	1.3383	2.5192	(3.3542)
log (R/R$_\odot$)	(-0.8257)	-0.5134	0.2709	0.9243	1.7330	(2.2593)
log T_e	(3.3710)	3.8270	3.7439	3.6360	3.5268	(3.4724)
X_s	(0.54054)	0.33096	0.47001	0.58958	0.69294	(0.68108)
M_{env}	(0.1000)	0.0318	0.0221	0.0149	0.0097	(0.0360)
log ($\mathscr{L}_\nu/\mathscr{L}_\odot$)	(——)	-5.6747	-4.3643	-3.3570	-1.6890	(-0.1726)
log T_{sh}	(6.6219)	7.2089	7.3337	7.4258	7.5616	(7.6559)
log ρ_{sh}	(2.3332)	2.8956	2.5554	2.2484	1.7655	(1.3066)
ψ_{sh}	(1.6938)	0.1148	-1.2688	-2.3421	-3.9131	(-5.1975)
log T_c	(6.6748)	7.2439	7.3773	7.4920	7.6958	(7.8895)
log ρ_c	(2.4104)	4.4771	4.9167	5.2185	5.5975	(5.8976)
ψ_c	(1.6933)	10.2245	14.6232	17.5861	19.0669	(18.6121)

(i) Ages are measured from the homogeneous main sequence.

(ii) The $0{\cdot}10\ M_\odot$ model refers to the core hydrogen-burning model of largest radius in the evolutionary sequence.

(iii) The $0{\cdot}50\ M_\odot$ model refers to the onset of the helium flash (specifically, to the onset of convection in a shell immediately above the helium-burning shell).

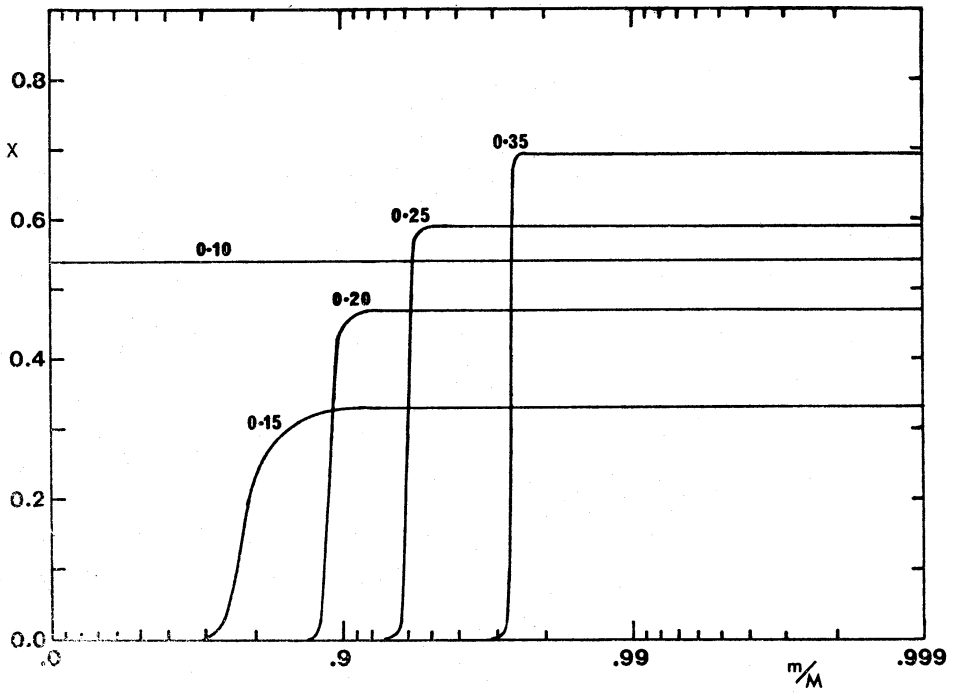

FIG. 1. *Composition profiles of zero-age remnants. The flat profile for the* 0·10 $M_\odot$ *star refers to the core hydrogen-burning-model of largest radius in the evolutionary sequence.*

where X and Y are the local hydrogen and helium abundances, respectively, and M is the total mass of the star. Fig. 1 shows the composition profiles of stars on the ZAR sequence.

Stars sufficiently massive to lift any shell degeneracy, $M \gtrsim 0{\cdot}17\ M_\odot$, support CNO-cycle shell burning. The least massive stars remain in degenerate p–p burning with very broad shells and large envelope masses. The model of 0·20 $M_\odot$ is an interesting hybrid in that p–p burning in the upper half of the shell is still a major energy source, though most of the luminosity comes from CNO-cycle burning, and the very bottom of the shell remains partially degenerate. Stars less massive than this have nearly isothermal cores, whereas stars sustaining CNO burning have larger temperature differences between centre and shell because of gravitational heating in the more rapidly growing cores. Neutrino losses only become significant near the upper limit to the mass range: in the 0·35 $M_\odot$ model they are sufficiently strong to create a core temperature inversion with maximum temperature, $\log T = 7{\cdot}7031$, at mass fraction $M/M_* = 0{\cdot}401$.

As the stars considered here are presumed to arise out of mass loss from more massive binary components, it is necessary then to restrict the scope of applicable binary remnants to those which are in the same thermal state as those evolving at constant mass up the giant branch. It is necessary then that the binary be evolving on a time scale longer than the thermal time scale of the primary's core. Thus these are stars arising out of Case A mass transfer, or Case B with low angular momentum, i.e. remnants in relatively short-period close binary systems.

4. EVOLUTION INTO THE WHITE DWARF REGION

The evolutionary tracks in the Hertzsprung–Russell diagram of the models considered here are plotted in Fig. 2. The salient properties of models at selected

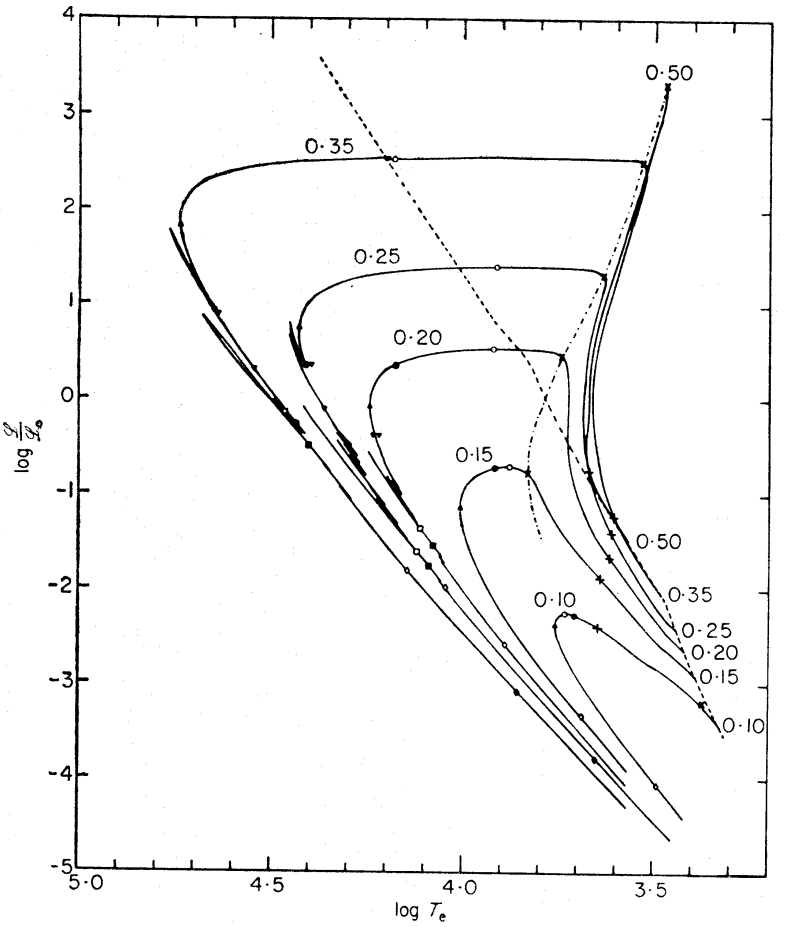

FIG. 2. *Evolutionary tracks of models in the Hertzsprung–Russell diagram, labelled by their respective masses in solar units. The homogeneous zero-age main sequence is indicated by a dashed line, the zero-age remnant sequence by a dash–dotted line. Epochs of interest are indicated by different symbols:* +, *central hydrogen exhaustion,* $X_c = 0{\cdot}001$; ×, *maximum radius (zero-age remnant: epoch A);* ○, *maximum shell temperature,* T_{sh} *(B);* ●, *maximum central temperature,* T_c *(C);* ▲, *maximum surface temperature,* T_e *(D);* ▽, ▼, *beginning and end of thermal pulse at onset of shell degeneracy* (E_1, E_2); □, ■, *beginning and end of thermal pulse at reversion to p–p shell burning* (F_1, F_2); ◇, T_c *drops to* $1/e$ *of its maximum value (G);* ◆, T_c *drops to* $1/e^2$ *of its maximum value (H).*

epochs are listed in Table II. Fig. 3 illustrates the thermal histories of the 0·15, 0·20, 0·25 and 0·35 $M_\odot$ models following turn-off. The evolution of these stars naturally falls into two phases, according to the type of hydrogen-burning in the shell, although both phases do not necessarily occur in all such stars.

4.1 *CNO-cycle shells*

Stars massive enough to sustain CNO-cycle shell burning have generally much smaller envelope masses when they leave the giant branch than less massive stars, with the envelope mass at turn-off decreasing roughly as $M^{-1{\cdot}28}$. Since the luminosity at turn-off increases approximately as the eighth power of the mass, the remaining envelope is very quickly burned away to such small mass that it can no longer maintain sufficient pressure to burn hydrogen non-degenerately in a CNO-cycle shell. Maximum shell temperature (Epoch B) is reached very quickly, and in the face of the rapidly dwindling mass and heat capacity of the envelope, the shell begins cooling rapidly and rising in degeneracy.

TABLE II

Epoch	Age (10^6 yr.)	log ($L/L_\odot$)	log ($R/R_\odot$)	log T_e	M_{env}	log ($L_\nu/L_\odot$)
			0.10 $M_\odot$			
C	4 253 233.	-2.2558	-1.0207	3.7099	0.0352	-7.7325
B	4 268 324.	-2.2387	-1.0567	3.7321	0.0298	-7.3448
D	4 300 343.	-2.3543	-1.1670	3.7585	0.0193	-6.8867
G	4 480 561.	-4.0417	-1.4743	3.4903	0.0072	—
			0.15 $M_\odot$			
B	3 352.0	-0.7093	-0.5984	3.8854	0.0213	-5.3941
C	3 664.9	-0.7206	-0.6526	3.9097	0.0193	-5.3552
D	5 992.5	-1.1339	-1.0527	4.0065	0.0106	-5.2979
G	51 818.	-3.3145	-1.5122	3.6910	0.0029	—
			0.20 $M_\odot$			
B	116.10	0.5453	-0.0329	3.9163	0.0138	-4.2071
C	202.19	0.3646	-0.6446	4.1770	0.0084	-4.0939
D	289.94	-0.0640	-0.9937	4.2445	0.0058	-4.1121
E	340.67	-0.3643	-1.1174	4.2312	0.0052	-4.1632
F_1	996.29	-1.3557	-1.3724	4.1108	0.0037	-4.8156
F_2	1 312.08	-1.5250	-1.3913	4.0779	0.0032	-4.6820
G	10 294.	-2.5719	-1.5364	3.8887	0.0019	—
			0.25 $M_\odot$			
B	17.656	1.4201	0.4140	3.9115	0.0077	-3.2293
D	33.888	0.7547	-0.9576	4.4310	0.0032	-3.1008
C, E_1	40.588	0.3427	-1.1279	4.4132	0.0028	-3.0908
E_2	48.643	-0.0863	-1.2472	4.3656	0.0025	-3.1070
F_1	573.59	-1.6184	-1.5157	4.1168	0.0019	-4.6932
F_2	899.66	-1.7376	-1.5214	4.0898	0.0015	-4.4506
G	1 513.8	-1.9939	-1.5562	4.0432	0.0015	-5.2187
H	24 026.	-3.7804	-1.6593	3.6481	0.0010	—
			0.35 $M_\odot$			
B	1.2663	2.5380	0.4315	4.1823	0.0031	-1.5993
D	1.8200	1.8364	-1.0378	4.7416	0.0011	-1.5561
E_1	2.0944	0.9318	-1.3027	4.6478	0.0010	-1.5418
E_2	2.7307	0.3192	-1.4119	4.5493	0.0009	-1.5299
C	6.1643	-0.2656	-1.4854	4.4398	0.0008	-1.5169
F_1	12.596	-0.1576	-1.4911	4.4697	0.0008	-1.5798
F_2	17.414	-0.5069	-1.5280	4.4008	0.0007	-1.6495
G	292.56	-1.7951	-1.6584	4.1440	0.0006	-4.0211
H	4 305.8	-3.0553	-1.7239	3.8617	0.0006	—

Epoch	log T_{sh}	log ρ_{sh}	ψ_{sh}	log T_c	log ρ_c	ψ_c
			0.10 $M_\odot$			
C	6.9967	2.9747	1.3591	7.0946	3.9408	6.2969
B	7.0217	3.0087	1.4410	7.0934	4.0471	7.4745
D	6.9997	3.0838	1.7879	7.0672	4.2544	10.9738
G	6.6406	3.2871	6.8619	6.6603	4.5612	44.8750
			0.15 $M_\odot$			
B	7.2205	2.9176	0.1217	7.2560	4.6011	12.0173
C	7.2199	2.9181	0.1345	7.2563	4.6232	12.4226
D	7.1721	3.0208	0.7179	7.2174	4.7664	16.8965
G	6.7998	3.2080	4.1912	6.8220	4.9477	55.2442
			0.20 $M_\odot$			
B	7.3481	2.5878	-1.2934	7.3950	4.9673	15.1432
C	7.3284	2.6239	-1.0639	7.4066	5.0154	15.8476
D	7.2923	2.8114	-0.4353	7.3916	5.0595	17.5243
E	7.2657	2.9330	0.0000	7.3754	5.0800	18.7538
F_1	7.1335	3.1003	1.1839	7.2154	5.1643	30.7691
F_2	7.1010	3.0825	1.3840	7.2399	5.1551	28.6797
G	6.9410	3.0213	3.2216	6.9723	5.2222	58.6927
			0.25 $M_\odot$			
B	7.4389	2.2650	-2.3893	7.5085	5.2483	17.6858
D	7.3739	2.5644	-1.3963	7.5267	5.2815	17.8094
C, E_1	7.3361	2.7607	-0.7683	7.5291	5.2907	17.9480
E_2	7.3006	3.0209	0.0187	7.5268	5.2989	18.2646
F_1	7.0866	3.1025	1.6652	7.1993	5.4239	46.6977
F_2	7.0617	3.0849	1.6772	7.2362	5.4144	42.3069
G	7.0368	3.2066	2.3313	7.0948	5.4414	60.9537
H	6.6417	3.4046	8.7462	6.6605	5.4775	174.6510
			0.35 $M_\odot$			
B	7.5837	1.8084	-3.9041	7.7078	5.6164	19.0540
D	7.4916	2.1874	-2.7343	7.7138	5.6261	19.0519
E_1	7.4075	2.7256	-1.2263	7.7158	5.6293	19.0521
E_2	7.3255	3.0292	-0.2549	7.7179	5.6329	19.0569
C	7.3057	3.2210	0.5557	7.7229	5.6457	19.1891
F_1	7.3113	3.1711	0.3898	7.7125	5.6618	20.1106
F_2	7.2791	3.2728	0.8504	7.6976	5.6719	21.1203
G	7.0820	3.3207	2.4772	7.2886	5.7907	64.1916
H	6.8236	3.4748	6.3118	6.8543	5.8260	183.4026

(i) Ages are measured from the zero-age remnant sequence (Table I).

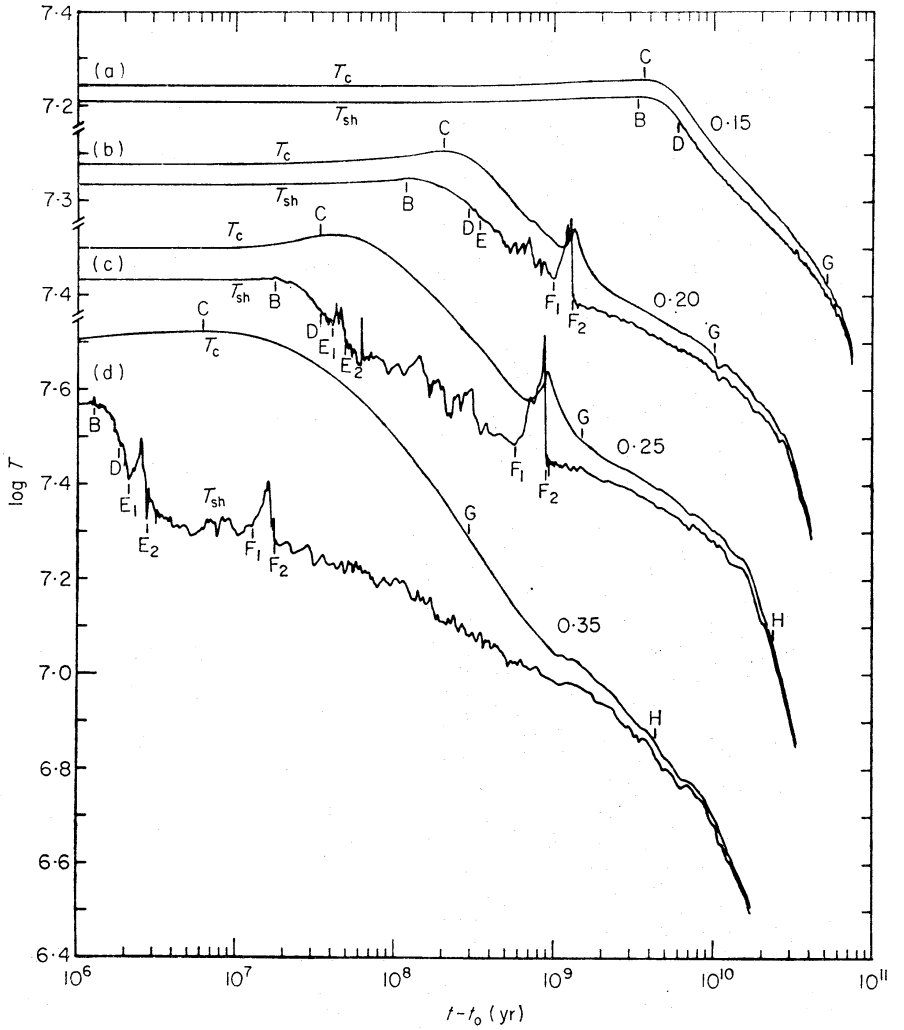

FIG. 3. *Thermal histories of central and shell temperatures for* (*a*) 0·15 $M_\odot$, (*b*) 0·20 $M_\odot$, (*c*) 0·25 $M_\odot$ *and* (*d*) 0·35 $M_\odot$ *models. Ages are measured from the zero-age remnant sequence. Note that the temperature scales are offset vertically.*

When the shell reaches approximately neutral degeneracy, $\psi_{sh} = 0$, a strong thermal pulse may occur (E_1–E_2 in Fig. 3(c) and (d)). Kippenhahn *et al.* (1968) found, in the study of a 0·264 $M_\odot$ white dwarf remnant of case B mass transfer, a slow increase in shell luminosity followed by two violent shell flashes. This distinct episode may be absent in the very lowest mass CNO-burning stars (E in Fig. 3(b)), as the shell never completely lifts degeneracy in those cases, and with a slower core growth rate during previous evolution, the core remains nearly isothermal with respect to the bottom of the shell, thereby resisting any attempt by the shell to cool quickly to complete degeneracy, setting off a thermal runaway. Runaway behaviour may be inhibited further by the more stable behaviour of the p–p burning upper portion of the shells of these lower mass stars. Unpublished calculations by the author of low-mass binary evolution in case A resulting in remnants of 0·2065 $M_\odot$ and 0·2078 $M_\odot$ seem to indicate that a distinct pulse probably first appears in the neighbourhood of 0·206 $M_\odot$.

The pulse, if it occurs, is followed by a relatively brief period of highly unstable partially degenerate CNO-cycle shell burning (Epochs E_2 to F_1). In this phase

20–60 per cent of the total luminosity of the star may come from gravitational contraction, the more massive stars deriving the larger fraction from this source. During this phase (and certainly during the partially degenerate p–p burning discussed below) the emerging importance of electron screening may offset to some extent the inclination of thin shells towards further runaways. From Schwarzschild & Härm (1965) and Bolton & Eggleton (1973), we know that the temperature sensitivity of nuclear burning is pivotal to its stability. In weak screening, this sensitivity may be buffered:

$$\left(\frac{\partial \ln \epsilon}{\partial \ln T}\right)_\rho \equiv \nu = \nu_0 - 1{\cdot}5 \ln f, \tag{3}$$

where ν_0 is the unscreened exponent and f is the screening factor ($\ln f < 1$ for weak screening).

The increasing importance of p–p burning in the upper part of the shell gradually broadens it between E_2 and F_1, but its increasing degeneracy finally insures, at F_1, that a strong thermal pulse develops. Fig. 4 illustrates the change in character of the shell during the pulse between F_1 and F_2 for the 0·25 $M_\odot$ model. A runaway situation briefly develops which lifts the degeneracy of the entire shell. For stars sufficiently low in mass that the shell cannot cool appreciably faster than the core, the temperature rise associated with this pulse is sufficiently high to propagate a thermal wave towards the core. This wave temporarily reverses the

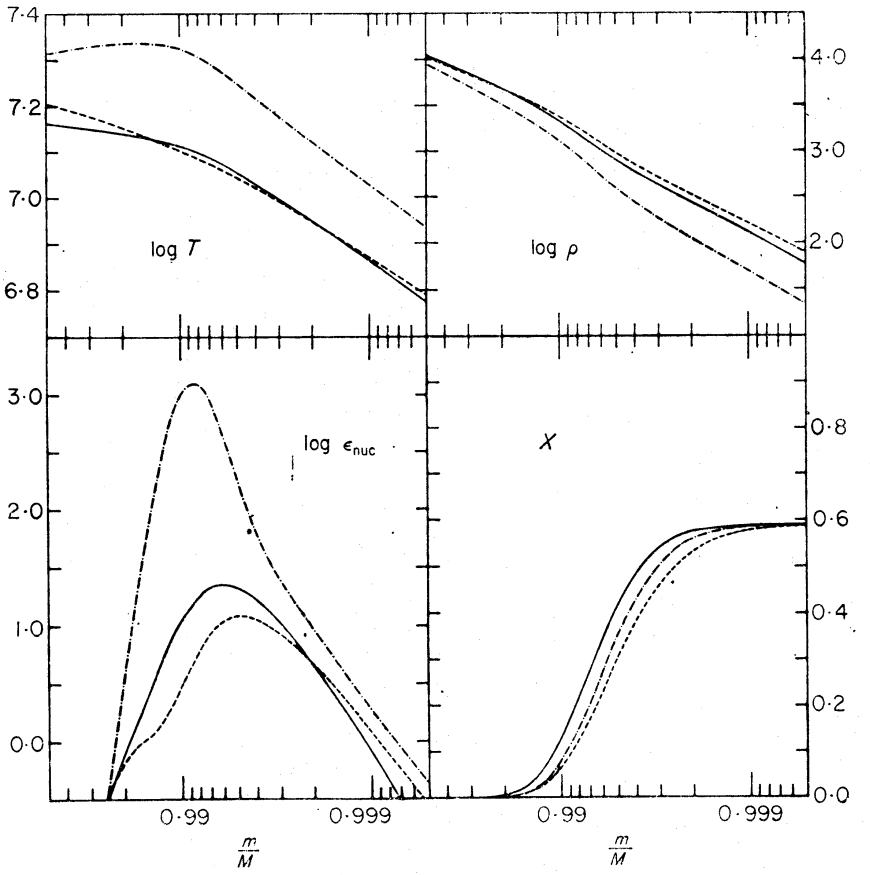

FIG. 4. *The thermal pulse in the 0·25 $M_\odot$ model at the reversion from CNO cycle to(p–p chain shell burning. The solid lines refer to epoch F_1, the dash–dotted lines to the peak of the pulse, and the dashed lines to epoch F_2.*

core contraction, and removes up to 1·6 per cent of the shell luminosity in the 0·25 $M_\odot$ star at maximum. The wave is seen arriving at the centre in Fig. 3(b) and (c) at an interval of the Kelvin–Helmholtz time scale for the entire star.

The pulse burns away enough of the remaining envelope that the collapse of the hydrogen-burning shell is only finally arrested by the onset of degenerate p–p shell burning. We see in Fig. 4 that a vestige of CNO burning remains, as a slight bulge on the lower end of the distribution of nuclear energy sources, but this quickly disappears as the shell cools further.

4.2 *p–p chain shells*

We noted before that shell-burning stars below $\sim 0{\cdot}17\ M_\odot$ cannot support the CNO cycle, and survive on p–p chain shell burning. The post-turn-off evolution of these stars (*cf.* Fig. 3(a)) is qualitatively similar, then, to the final p–p chain burning phase of more massive stars, except that given their far more massive envelopes, their evolution proceeds on an exceedingly long time scale, cosmologically insignificant much below about 0·15 $M_\odot$. Except for a thermal relaxation period following the CNO shell-burning phase described above, and the extinction of the shell much later, p–p chain burning supplies upwards of 90 per cent of the total stellar luminosity (as much as 98 per cent or more for the 0·15 $M_\odot$ star).

Although the hydrogen-burning shell is moderately degenerate throughout this phase of evolution, thermal instabilities such as one might expect in such a regime (Mestel 1952) never develop to very large amplitude. We may understand this merely as reflecting (a) the low degree of degeneracy, in which the pressure and density of shell material is still moderately sensitive to temperature; (b) the large fraction of the envelope, mass-wise, contained within the burning region, meaning that the growth time for burning instabilities and relaxation time scale of the envelope differ so little that thermal runaways cannot develop; and (c) as we have seen above, electron screening can be important in moderating the temperature-dependence of nuclear reaction rates, especially when the unscreened rates are already relatively weakly temperature-sensitive.

5. DEATH OF THE HYDROGEN-BURNING SHELL

There exists some envelope mass small enough for a star of given total mass, which will no longer sustain the p–p shell-burning stage reached by all stars in this study. Stars gradually come to rely more heavily on gravitational contraction as a source of energy and the evolutionary time scale decreases to the cooling time scale for the core. We have indicated at epochs G and H the times at which the central temperature has fallen by e and e^2, respectively, from maximum at C.

As the shell cools towards extinction, the surface convective zone engulfs a great part of the mass of the remaining envelope above the shell. Present calculations were stopped when pressure ionization effects began to dominate the structure of the envelope. In the region of pressure ionization a barrier is built up which prevents the convective envelope from reaching into regions of nuclear burning and hence composition gradients. At higher pressures, $\nabla_{ad} \simeq 0{\cdot}4$ and the opacity is relatively low; at lower pressures, $\nabla_{ad} < 0{\cdot}4$ and bound–free absorption drives the opacity to high values stimulating convection. In the region of pressure ionization itself, increasing density depresses the ionization continuum, effectively reducing the ionization potential of atomic species. Since the degree of ionization is princi-

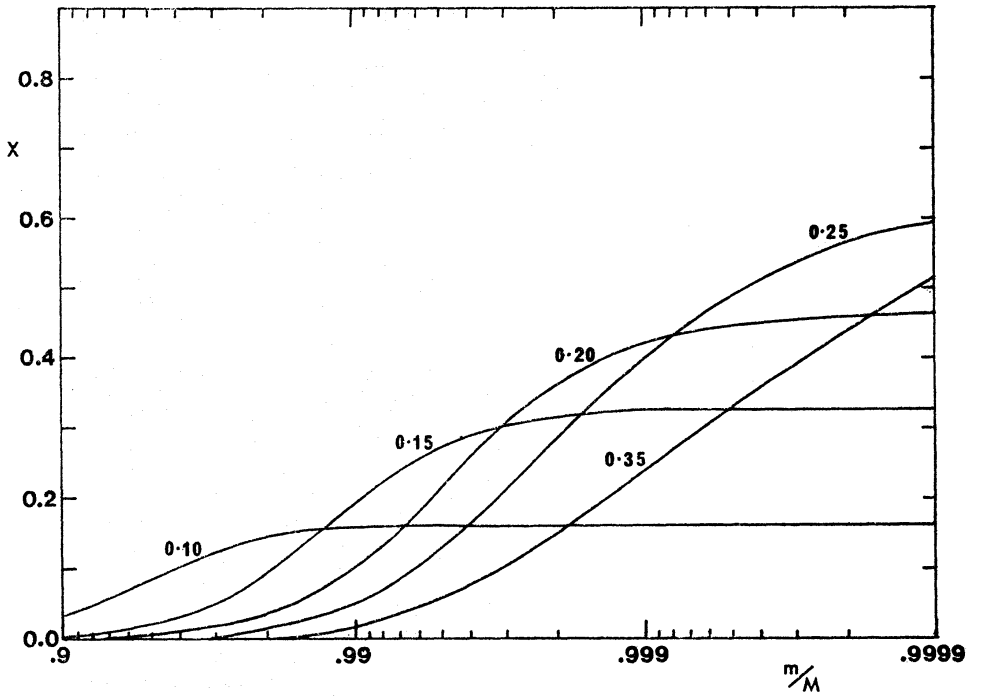

FIG. 5. *Composition profiles in models at the end of the evolutionary sequences.*

pally a function of the electron density and the ratio of the effective ionization potential to mean kinetic energy, for sufficiently high density the degree of ionization will depend more strongly upon variations in continuum depression (primarily a function of density) than on variations in mean kinetic energy (function of temperature), provided that the latter is small compared with the vacuum ionization potential. Since the entropy of the gas is most strongly dependent upon the number densities of particles of different species, it is clear that the entropy will become more strongly density-dependent than in the case of constant numbers of particles. Thus ∇_{ad} increases in pressure-sensitive regions, whereas in the usual temperature-dominated regime ∇_{ad} is depressed. At the termination of the present sequences, the maximum values were typically $\nabla_{ad} \simeq 0{\cdot}6$.

Presumably further calculations would have shown that this zone gradually then acquires the characteristics of a sharp phase transition between completely unionized and completely ionized gases at low temperatures. Fig. 5 shows the fossil composition profiles resulting from the present calculations.

6. WHITE DWARF POPULATIONS IN CLOSE BINARY SYSTEMS

Fig. 6 shows a set of isochrones constructed from the evolutionary sequences presented here, with ages again referred to the ZAR sequence. Isochrones have also been plotted for eras preceding the sequence. These would correspond to systems still in a semi-detached configuration and are therefore not strictly applicable, as the mass is then variable. We do observe, however, that, as one expects, giant branch evolution is largely independent of the total mass of the star. For negative ages, the vast majority of semi-detached red giants lie along the short horizontal segments of the isochrones, with only those stars already leaving the branch scattered along the long tail paralleling the giant branch. With some certainty, then, one can infer the

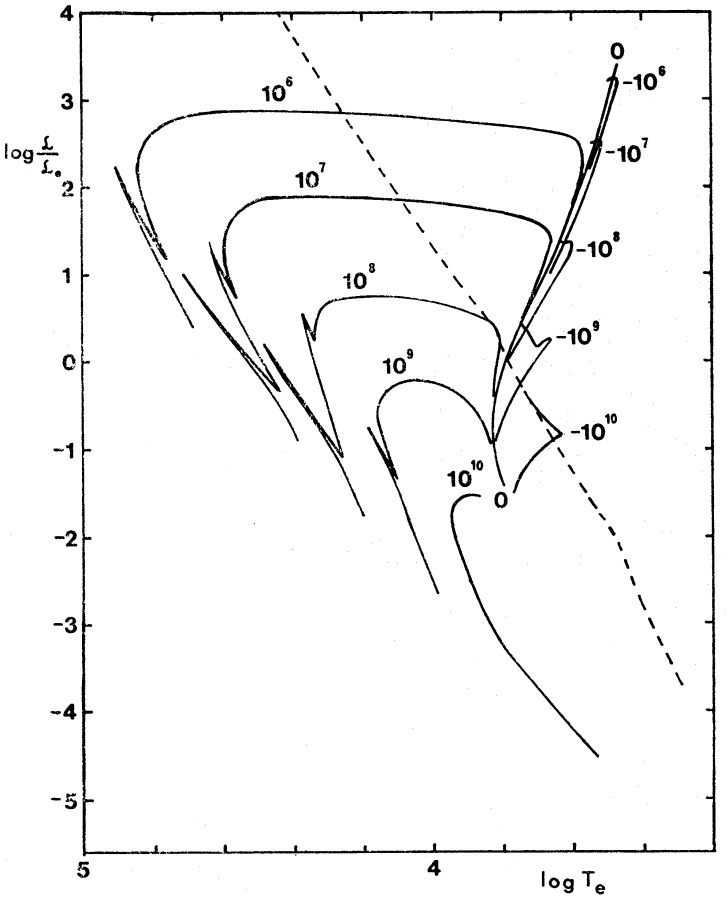

FIG. 6. *Isochrones for the present model sequences referred to the zero-age remnant sequence. The dashed line marks the homogeneous zero-age main sequence.*

future duration of a semi-detached system transferring mass on a nuclear time scale merely from the present luminosity of the red giant component. We can, in turn, rule out any possibility of forming white dwarfs less massive than $\sim 0{\cdot}15\ M_\odot$ by mass transfer within any acceptable time scale: in cases applicable here the final stages of evolution leading to detachment become impossibly slow, whereas systems with larger initial separations necessarily develop larger cores before initiating mass transfer.

One could in principle use the isochrones for positive ages to determine with some accuracy the time elapsed since a system observed to have a white dwarf became detached, or at least a minimum such age for a system observed to be in an active phase of mass transfer. In fact, comparison with Fig. 2 shows that, in the region between the red giant and white dwarf tracks, the total luminosity of a star is fixed to a very high degree by its total mass, a notoriously elusive parameter in the solution of light curves. The mass and age of such a remnant might then be well established. Unfortunately, for stars already on the white dwarf track, thermal instabilities, smoothed out in Fig. 6 except for the episodes E_1–E_2 and F_1–F_2, hopelessly tangle the isochrones, leaving the age defined only within a factor of two even with perfectly determined masses.

It should be noted that for the most massive stars of the type modelled here, time scales preceding epoch E may be systematically overestimated compared with remnants from close binary mass transfer. Stars with extensive convective envelopes

on the upper part of the giant branch may have smaller envelope masses when they become detached than implied by the present study, as mass transfer tends to expand a convective envelope relative to thermal equilibrium (Lauterborn & Weigert 1972), keeping the system in mass transfer longer than otherwise would be expected, and significantly reducing the initial envelope mass of the remnant.

With regard to accreting white dwarfs as models of novae, one may reasonably suppose that only in the time span between epochs A (zero-age remnant) and B (maximum shell temperature), when the shell temperature differs little from a stable shell in a more massive star of the same core mass, is accretion likely to lead directly to reversion to the giant branch without nova-like outbursts. At later stages of evolution, we can expect that any accretion rate which compresses the envelope more rapidly than it relaxes thermally will certainly lead to a nova outburst. The thermal relaxation time scale for the envelope is:

$$\tau_{\rm env} \simeq \frac{GMM_{\rm env}}{\mathscr{L}R}. \tag{4}$$

The upper limit for quiescent mass accretion is then:

$$\dot{M} < \frac{M_{\rm env}}{\tau_{\rm env}} \simeq 3{\cdot}24 \times 10^{-8} \left(\frac{\mathscr{L}}{\mathscr{L}_\odot}\right)\left(\frac{R}{R_\odot}\right)\left(\frac{M}{M_\odot}\right)^{-1} M_\odot \ {\rm yr}^{-1}. \tag{5}$$

Certainly for any epoch beyond E, this mass transfer rate will easily be exceeded in the early (thermal time scale) phases of any second period of mass transfer.

7. CONCLUSION

It will be noted that in none of the model sequences presented here was such a severe thermal runaway as described by Kippenhahn *et al.* (1968) observed. Throughout the present study, the time steps used in computing sequences were of the order of 0·2 $\tau_{\rm env}$ to 1·0 $\tau_{\rm env}$. No thermal instability can have a growth or decay time appreciably longer than $\tau_{\rm env}$; on the other hand, any instabilities with growth or decay times significantly shorter than the time step will be numerically suppressed. As aptly pointed out by Schwarzschild & Härm (1965), the existence of thermal runaways may never surface under these conditions. On the other hand it is clear from the present study that a great deal of mode-mixing occurs in the thermal instabilities which persist throughout the white dwarf stage, so that the problem only becomes manageable if all but the longest-period instabilities are suppressed. The danger exists, of course, that non-linear effects (such as convection, in particular) in the suppressed instabilities may alter the long-term course of evolution. One can only conjecture at present what such effects might be, but we note that the model of Kippenhahn *et al.* (1968), at the end of the thermal pulse, does not differ greatly from that expected at E_2 in the present study.

Finally, we note that the present results may be partially stabilized by two spurious influences. First, the use of a non-Lagrangian mesh inevitably entails some numerical broadening of a composition profile during a thermal pulse (Eggleton 1972), the broadened shell being less susceptible to a runaway. Secondly, the use of weak-screening factors under conditions late in CNO and p–p shell burning when intermediate or strong screening is applicable leads to systematic overestimation of shell-luminosities (possibly prolonging the relevant phases of

evolution), and underestimation of the temperature dependence of the reaction rates under the given conditions.

ACKNOWLEDGMENTS

The author gratefully acknowledges the invaluable aid of P. P. Eggleton and useful discussions with R. T. Rood. The author was supported during this research by a scholarship awarded by the Marshall Aid Commemoration Commission, London.

REFERENCES

Bolton, A. J. C. & Eggleton, P. P., 1973. *Astr. Astrophys.*, **24,** 429.
Eggleton, P. P., 1971. *Mon. Not. R. astr. Soc.*, **151,** 351.
Eggleton, P. P., 1972. *Mon. Not. R. astr. Soc.*, **156,** 361.
Eggleton, P. P., Faulkner, J. & Flannery, B. P., 1973. *Astr. Astrophys.*, **23,** 325.
Frank-Kamenetskii, D., 1962. *Physical processes in stellar interiors*, Israel Program for Scientific Translations, Jerusalem, transl. from the Russian (*Fizicheskie Protsessy Vnutri Zvezd*, Gos. izdat. fiz.-mat. lit., Moscow, 1959), Ch. 7, p. 177.
Kippenhahn, R., Thomas, H.-C. & Weigert, A., 1968. *Z. Astrophys.*, **69,** 265.
Kovetz, A. & Shaviv, G., 1970. *Astr. Astrophys.*, **8,** 398.
Lauterborn, D. & Weigert, A., 1972. *Astr. Astrophys.*, **18,** 294.
Mestel, L., 1952. *Mon. Not. R. astr. Soc.*, **112,** 583.
Refsdal, S. & Weigert, A., 1970. *Astr. Astrophys.*, **6,** 426.
Refsdal, S. & Weigert, A., 1971. *Astr. Astrophys.*, **13,** 367.
Rose, W. K., 1972. *Stellar evolution*, p. 289, eds H.-Y. Chiu & A. Muriel, M.I.T. Press, Cambridge, Mass., London.
Schwarzschild, M. & Härm, R., 1965. *Astrophys. J.*, **142,** 855.
Ziolkowski, J., 1970. *Acta Astr.*, **20,** 213.